Available online at www.sciencedirect.com
SCIENCE DIRECT
Polymer 47 (2006) 4734–4741
polymer
www.elsevier.com/locate/polymer

Polymer nanotube nanocomposites: Correlating intermolecular interaction to ultimate properties

Asif Rasheed [a], Han Gi Chae [b], Satish Kumar [b], Mark D. Dadmun [a,c,*]

[a] Department of Chemistry, University of Tennessee, 323 Buehler Hall, Knoxville, TN, USA
[b] School of Polymer, Textile and Fiber Engineering, Georgia Institute of Technology, Atlanta, GA, USA
[c] Chemical Sciences Division, Oak Ridge National Laboratory, Oak Ridge, TN, USA

Received 7 February 2006; received in revised form 4 April 2006; accepted 5 April 2006
Available online 19 May 2006

Abstract

Polymer nanocomposite films containing 5 wt% single-walled carbon nanotubes (SWNT) or 5 wt% multi-walled carbon nanotubes (MWNT) with random copolymers of styrene and vinyl phenol were processed from dimethyl formamide solutions. Vinyl phenol mole ratio in the copolymer was 0, 10, 20, 30, and 40%. FTIR analysis indicates that the composites containing the copolymer with 20% vinyl phenol exhibit the maximum intermolecular interactions (hydrogen bonding) between the hydroxyl group of the vinyl phenol and the carbon nanotube functional groups. Tensile properties and electrical conductivity also are the highest in the samples containing the copolymer with 20% vinyl phenol. Thus, these results show that the optimization of the extent of intermolecular interactions between a polymer chain and a carbon nanotube results in an optimal increase in macroscopic properties. Moreover, the extent of intermolecular hydrogen bonding can be improved by optimizing the accessibility of the functional groups to participate in the non-covalent interaction. In this system, this optimization is realized by control of the amount of vinyl phenol in the copolymer, i.e. the copolymer composition.

Keywords: Carbon nanotube; Polymer nanocomposite; Intermolecular interaction

1. Introduction

Carbon nanotubes (CNT) have emerged as a promising class of materials that possess extraordinary mechanical and electrical properties [1–4]. Significant attention is being given to achieving a homogenous dispersion of CNT in a polymer matrix, as such a composite promises a novel material with significantly enhanced properties [5–9]. The extent of property enhancement of such a nanotube polymer nanocomposite depends on a number of factors; two of the most important are the extent of nanotube dispersion in the polymer matrix and the interaction between the nanotubes and the host polymer. A homogeneous, uniform dispersion of the nanotubes in the polymer matrix, with significant interactions between them, is desirable in creating an optimal nanocomposite. The nanotubes exfoliation into a polymer matrix and its effect on mechanical properties has been reported [10]. The importance of the interaction between the polymer and the nanotubes has been demonstrated in terms of the ultimate mechanical properties of composites [11–14], shifts in characteristic peaks in Raman spectra [15–21] and wetting of the nanotubes with polymer as observed by transmission electron microscopy (TEM) [1,22]. However, attempts to quantify the amount of the interaction between the nanotube and polymer matrix using these techniques have not been reported. Quantification of a polymer–nanotube interaction by detaching an individual nanotube from a polymer matrix using a scanning probe microscopy (SPM) tip [23] and atomic force microscopy (AFM) tip [24] and measurement of adhesion between nanotubes paper and modified AFM tip [25,26] has been reported.

The miscibility in amorphous polymer blends that interact via hydrogen bond has been widely studied [27–34]. It has been found that the control of the miscibility window of the blend depends upon the extent of interaction between the blend components. A similar approach has been employed to create miscible blends of an amorphous and a liquid crystalline polymer [35–39]. The hydrogen bond interaction responsible for inducing miscibility in polymer blend systems has been

* Corresponding author. Address: Department of Chemistry, University of Tennessee, 323 Buehler Hall, Knoxville, TN 37996-1600, USA. Tel.: +1 865 974 6582.
E-mail address: dad@utk.edu (M.D. Dadmun).

0032-3861/$ - see front matter © 2006 Elsevier Ltd. All rights reserved.
doi:10.1016/j.polymer.2006.04.016

investigated [27,29–31,33,36,38,39] and in certain cases quantified using infrared spectroscopy [29,31,33,36,38].

Carbon nanotubes contain structural defects [40] as well as oxidized carbon sites [41]. The structural defects include kinks, dangling bonds, dislocations, and 5,7 ring defects, whereas the oxygenated functional groups contain carbonyls, carboxylic acids and other oxygenated functional groups. The oxygenated functional groups on the nanotube ends and surface are potential sites for interaction with a polymer via hydrogen bond.

As improving and optimizing the extent of hydrogen bonding between two components is known to increase the level of dispersion and miscibility in a polymer blend, the role of hydrogen bonding in improving and controlling the dispersion of polymer nanocomposites is intriguing. Can the same principles that are known to apply to polymer blends be applied to polymer nanocomposites? To answer this question, polymer–carbon nanotube intermolecular interactions have been systematically varied and documented using infrared spectroscopy. This variation in intermolecular interaction is then correlated to the structural properties of the resultant nanocomposite. Single-walled carbon nanotubes (SWNT) and multi-walled carbon nanotubes (MWNT) are utilized to prepare nanocomposites with copolymers of styrene and vinyl phenol, poly(styrene-*co*-vinyl phenol) (PSVPh) containing 0, 10, 20, 30, and 40% vinyl phenol.

2. Experimental

2.1. Materials

Styrene and 4-acetoxystyrene monomers used for polymer synthesis, the initiator 2,2′-azobisisobutyronitirle (AIBN), solvents for copolymer synthesis and composite preparation: *N*,*N*-dimethylformamide (DMF), methanol and hexane were obtained from Sigma–Aldrich and utilized without any further treatment. 1,4-Dioxane was purchased from Fisher Scientific.

SWNT prepared by HiPCO (~1.1% metal impurities) are received from Carbon Nanotechnologies, Inc. and used without further treatment. MWNT (prepared by CVD, containing <1% metal impurities) are obtained from Iljin Nanotech, Co. (Korea).

2.2. Polymer synthesis

Synthesis of the copolymers of styrene and vinyl phenol (PSVPh) was carried out by free radical polymerization of styrene and 4-acetoxystyrene monomers in appropriate amounts, using AIBN as the initiator and 1,4-dioxane solvent. The reaction mixture was stirred at 65 °C for 20 h under mild argon flow. The resulting copolymer was precipitated in cold methanol. The copolymer's composition was determined using nuclear magnetic resonance (NMR). The acetoxystyrene groups of the copolymer were converted to vinyl phenol groups by hydrolysis using hydrazine hydrate in dioxane. The hydrolyzed copolymer (PSVPh) was precipitated using cold methanol for the copolymer with 10 and 20% vinyl phenol and using hexane for the copolymer with 30 and 40% vinyl phenol. The completion of the hydrolysis reaction was confirmed by the disappearance of the acetoxy peak as indicated by NMR. The copolymers with 10, 20, 30, and 40% vinyl phenol content are designated as PSVPh10, PSVPh20, PSVPh30, and PSVPh40, respectively. The exact copolymer compositions with their molecular weights (before and after hydrolysis) and polydispersity index are listed in Table 1.

Table 1
Polymers synthesized for this work

	% Vinyl phenol	% Vinyl phenol actual[a]	Before hydrolysis	After hydrolysis	
			M_n (g/mol)[b]	M_n (g/mol)[b]	PDI
PS	0	0		105,840	1.6
PSVPh10	10	13.2	129,000	118,000	1.8
PSVPh20	20	19.0	116,000	108,000	1.9
PSVPh30	30	32.5		105,000	2.4
PSVPh40	40	42.0	123,000	116,900	2.2

[a] Determined by NMR.
[b] Measured by GPC.

2.3. Composite preparation

12.5 mg of SWNT was dispersed in 100 ml of DMF by sonication in a sonic bath (Branson 3510, 40 kHz) for 24 h. 237.5 mg of polymer was added to the SWNT/DMF dispersion and stirred at 70 °C until sufficient amount of solvent evaporated and the volume of dispersion reduced to 25 ml. Homogenous dispersion of the polymer and nanotubes was assisted by using an homogenizer (Bio Homogenizer by ESGE) for 5–10 min. The polymer/SWNT/DMF dispersion was than cast on a hot glass substrate (~60–65 °C). After solvent evaporation, the composite film was peeled off the glass substrate and further dried under vacuum at 90 °C for 1 day to ensure complete solvent removal. The MWNT composites were prepared using the same procedure. All composite samples contain 5% by weight nanotubes.

2.4. Characterization

Tensile tests were performed on an RSA III by Rheometric Scientific, where tensile strength, tensile modulus and strain were obtained from these measurements. The gauge length and crosshead speed for the tests were 10 mm and 0.05 mm/s, respectively. Ten strips (2 mm wide, 25 μm thick) of polymers and composite films were tested in each sample. The results for each sample were averaged, normalized to the tensile properties of the pure copolymer and plotted as a function of the copolymer composition. Tensile results for each copolymer and its composite were normalized to the tensile properties of the pure copolymer in order to eliminate molecular weight and composition effects. Electrical conductivity was measured using the four-probe method.

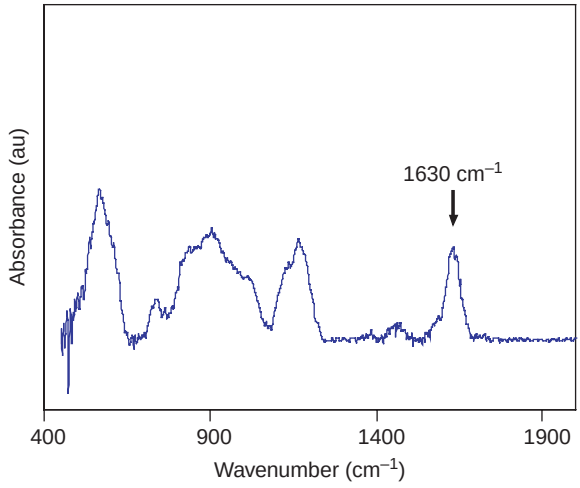

Fig. 1. FTIR spectra of SWNT.

FTIR spectra were collected by a spectrum one FTIR spectrometer by Perkin–Elmer. SWNTs were mixed with KBr powder and compressed as pellets for data collection. The spectrum was collected against KBr background. The copolymer and the nanocomposites were analyzed as films and the spectra were collected against air background. The FTIR spectra for polymer and nanocomposite films were collected as absorbance spectra using 64 scans at 2 cm^{-1} resolution. The FTIR spectrum of SWNT is given in Fig. 1. The peak at 1630 cm^{-1} in the FTIR spectrum indicates the presence of significant carbonyl groups in the as received purified SWNTs [42]. SWNT are also characterized by Raman spectroscopy and thermal gravimetric analysis (TGA) shown in Figs. 2 and 3, respectively. The D-band ($\sim$1330 cm^{-1}) in the Raman spectrum of SWNT indicates the presence of defects on the tubes. The combination of the presence of this Raman peak, the peak at 1630 cm^{-1} in the FTIR spectra, and the single peak in the temperature versus weight derivative (wt%/°C) curve of the SWNT TGA strongly indicate that oxygenated defects exist on the SWNT used in this study.

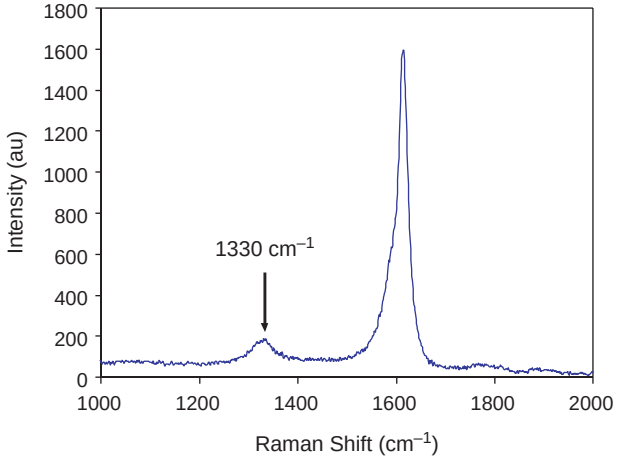

Fig. 2. Raman spectrum of SWNT.

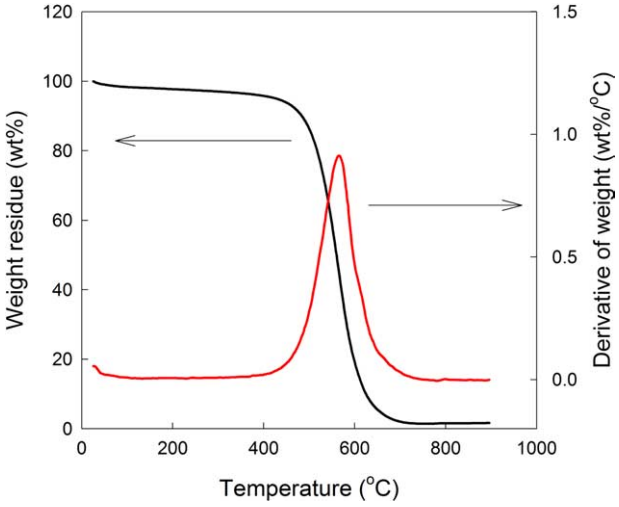

Fig. 3. TGA of as received SWNT.

3. Results

3.1. Tensile test

The tensile test results, given in Table 2, and the normalized tensile test results plotted in Figs. 4 and 5 show that for both, MWNTs and SWNTs, the maximum improvement in the composite tensile properties are observed for the 20% vinyl phenol containing samples. In general, tensile strength of the PSVPh10, PSVPh20, and PSVPh30 SWNT composites showed enhancement, while the nanocomposites of PS and PSVPh40 suffered a loss in strength. It is clear from Fig. 4 that the tensile strength of the composite increases as the PS is modified to PSVPh10 by incorporation of –OH groups that can interact with functional groups on the carbon nanotube, and this interaction increases further as the copolymer is modified to include 20% hydroxyl groups. This interaction, however,

Table 2
Summary of tensile results: polymer–SWNT and polymer–MWNT composites

% Vinyl phenol	PSVPh	PSVPh–SWNT (%increase/ decrease)	PSVPh–MWNT (%increase/ decrease)
Tensile strength (MPa)			
0	16±4	14±2 (−16%)	12±2 (−23%)
10	21±4	21±4 (2.4%)	20±8 (−2%)
20	20±3	27±5 (32%)	26±6 (30%)
30	21±4	23±4 (10%)	24±8 (11%)
40	27±4	16±4 (−42%)	24±3 (−10%)
Tensile modulus (GPa)			
0	1.5±0.3	2.0±0.2 (34%)	1.9±0.2 (33%)
10	1.7±0.3	2.6±0.4 (57%)	1.9±0.4 (16%)
20	1.6±0.3	2.9±0.3 (84%)	2.2±0.2 (39%)
30	1.9±0.3	2.8±0.4 (47%)	2.7±0.4 (43%)
40	2.1±0.2	2.0±0.5 (−2.8%)	2.7±0.3 (32%)
Strain to failure (%)			
0	1.5±0.4	0.8±0.2 (−44%)	0.7±0.2 (−54%)
10	1.6±0.3	0.9±0.2 (−42%)	1.2±0.3 (−27%)
20	1.3±0.2	1.2±0.2 (−6%)	1.4±0.4 (6%)
30	1.2±0.1	0.9±0.2 (−25%)	1.0±0.3 (−20%)
40	1.5±0.1	0.7±0.1 (−54%)	1.0±0.1 (−36%)

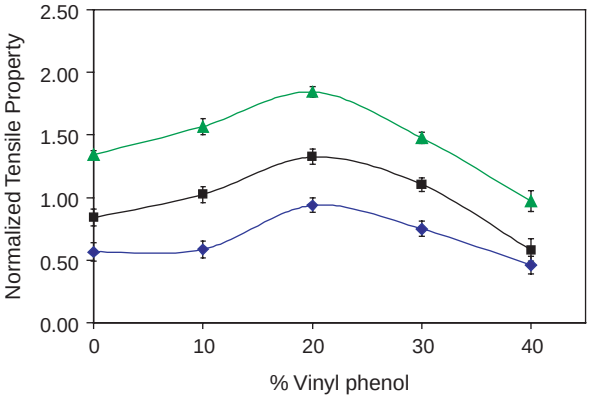

Fig. 4. Normalized tensile strength (■), tensile modulus (▲) and strain to failure (♦) versus % vinyl phenol for PSVPh–SWNT composites.

decreases as further hydroxyl groups are incorporated in the polymer chain (PSVPh30 and PSVPh40). The trend for dependence of the tensile modulus and strain to failure on the copolymer composition is similar to that of the tensile strength, however, the strain to failure decreased for all SWNT composites as compared to that of the pure copolymer. The tensile strength and strain to failure of the MWNT nanocomposites exhibited similar trends to the copolymer–SWNT composites, whereas no clear trend for the tensile modulus was observed.

3.2. Electrical conductivity of nanocomposites

The dc electrical conductivity of the nanocomposites for both SWNT and MWNT composites was also highest for the 20% vinyl phenol sample, as shown in Fig. 6. The electrical conductivity of a polymer–carbon nanotubes composite depends on a number of factors including nanotubes loading, nanotubes length, as well as their dispersion and exfoliation state. A higher value of electrical conductivity corresponds to well dispersed nanotubes in the polymer matrix [43], provided all other variables remain unchanged. Thus, based on the electrical conductivity of these samples, we conclude that

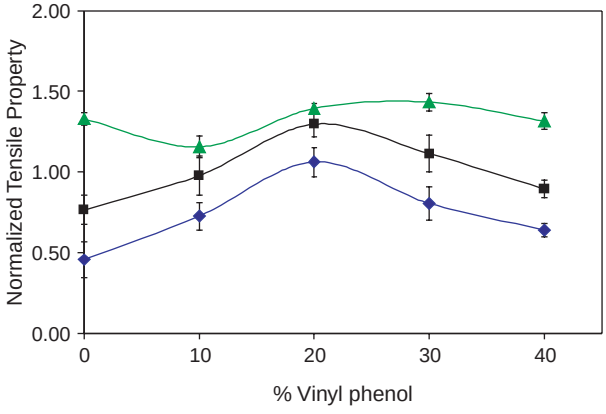

Fig. 5. Normalized tensile strength (■), tensile modulus (▲) and strain to failure (♦) versus % vinyl phenol for PSVPh–MWNT composites.

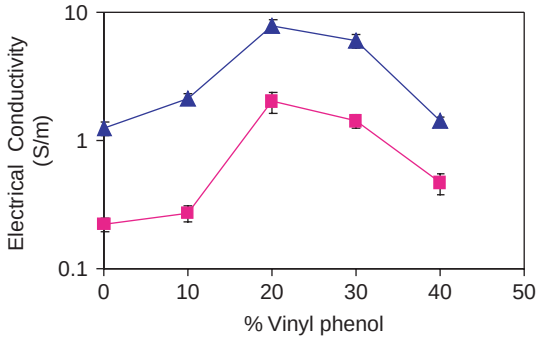

Fig. 6. Electrical conductivity of polymer composites as a function of polymer composition for SWNT composites (▲) and MWNT composites (■).

among the polymer samples studied, the PSVPh20 nanocomposite attained the best dispersion of the SWNT and MWNT.

3.3. FTIR spectra of the nanocomposites

FTIR spectra of the PSVPh copolymers in the hydroxyl stretching region (~3200–3600 cm^{-1}) and their composites with SWNT are plotted in Fig. 7. All spectra indicate that the hydroxyl group (–OH) of vinyl phenol exists as unassociated –OH groups (~3540 cm^{-1}) and associated (hydrogen bonded) –OH groups (~3400 cm^{-1}).

In these polymer–nanotube nanocomposites, some of the hydroxyl groups of PSVPh copolymer can interact with the oxygenated defect sites on the carbon nanotube via hydrogen bonding [40,41]. Hence, the associated –OH groups in the polymer–nanotube composites are comprised of –OH groups associated with another –OH on the polymer chain, an interaction that we will term intra-association, and –OH hydrogen bonding with the oxygenated functional groups of the nanotube, an interaction that we will term inter-association. The FTIR spectra, is analyzed to extract the contribution of the free –OH, the inter-associating –OH, and the intra-associating –OH to the measured spectra.

3.4. FTIR data analysis

The spectrum of the SWNT indicates the presence of carbonyl functional groups (Fig. 1); however, in the PSVPh–SWNT composites, the carbonyl (~1630 cm^{-1}) band is sufficiently diluted due to the low SWNT concentration (5 wt%) to make its analysis impractical. Thus, in order to determine the role of polymer–nanotube hydrogen bonding on the ultimate properties of these nanocomposites, the –OH stretching region of the spectrum must be analyzed. It must be noted that a quantitative analysis of the hydroxyl region is inherently difficult due to the vibration overlap of inter- and intra-molecular hydrogen bond association and overtones of the carbonyl group [29,33]. Hence, the analysis that follows, resolving the vibration bands into free and associated –OH and analyzing these ‘separate’ peaks to quantify the amount of each state of the hydroxyl group present (free versus hydrogen bonded) does not provide absolute concentrations.

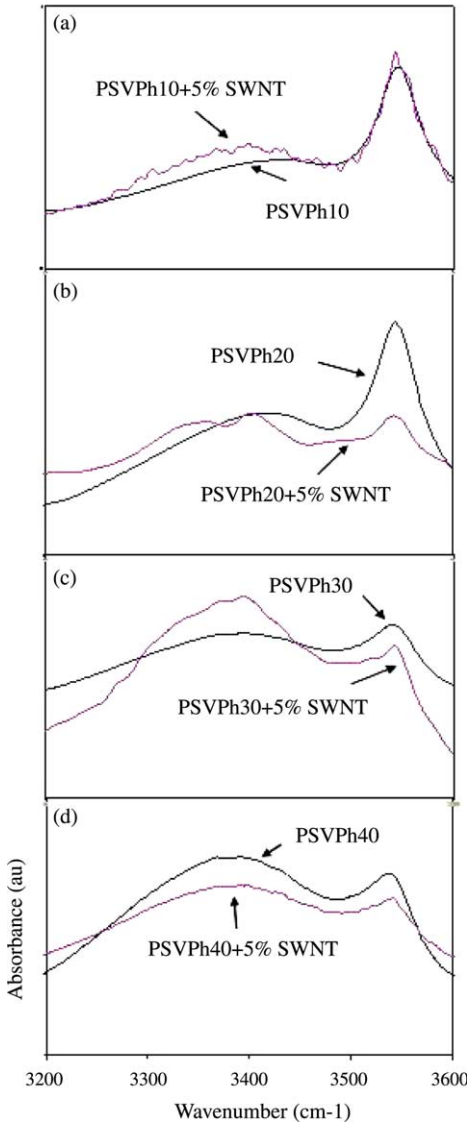

Fig. 7. FTIR spectra of pure copolymers and their composites with SWNT (a) PSVPh10 and PSVPh10+5%SWNT, (b) PSVPh20 and PSVPh20+5%SWNT, (c) PSVPh30 and PSVPh30+5%SWNT and (d) PSVPh40 and PSVPh40+5%SWNT in the region of –OH vibration.

The analysis, however, can be carefully used to document the relative change in the contribution of the free or hydrogen bonded –OH to the state of the system among a series of similar samples. Thus, this analysis is semi-quantitative, but will provide insight into the role of intermolecular association between carbon nanotubes and the surrounding polymer matrix on the engineering properties of these nanocomposites.

PeakFit v4.11 software was used to analyze the –OH bond stretching region in the FTIR spectra. In all fitting procedures, a Gaussian band shape was assumed. The –OH region between 3700 and 3100 cm^{-1} was resolved into free and associated –OH groups. During this deconvolution process in the analysis of the nanocomposites, the position and the width of the free and intra-associated hydrogen bonded –OH groups were fixed at those observed for the pure copolymer. The position and the width of the inter-associated –OH were allowed to vary in the fitting process.

The absorbance of a given vibration can be quantified using Beer–Lambert's law according to

$$A = abC \tag{1}$$

where A is the absorbance of a given vibration, a is its absorption coefficient, b is the path length or the sample thickness, and C is the concentration of the vibration group in the sample. The total concentration of –OH in the copolymer and the composite can be expressed as

$$C_{\mathrm{T,–OH}} = C_{\mathrm{F,–OH}} + C_{\mathrm{asso,–OH}} \tag{2}$$

where $C_{\mathrm{T,–OH}}$ is the total –OH concentration, $C_{\mathrm{F,–OH}}$ is the concentration of free –OH groups and $C_{\mathrm{asso,–OH}}$ is the concentration of –OH that participate in hydrogen bonding. The total –OH concentration in the sample can be calculated from

$$C_{\mathrm{T,–OH}} = \frac{dwf_{\mathrm{VPh}}}{M} \tag{3}$$

where d is the polymer density, w is the weight fraction of polymer in the system, f_{VPh}, is the molar fraction of vinyl phenol present in the copolymer and M is the molecular weight of vinyl phenol repeat unit. The concentration of free OH is calculated using Eq. (1) in the form

$$C_{\mathrm{F,–OH}} = \frac{A_{\mathrm{F,–OH}}}{(a_{\mathrm{F,–OH}}b)} \tag{4}$$

The concentration of associated –OH is obtained by subtracting the concentration of free –OH from the total concentration of –OH. In Eq. (4), the absorption coefficient for the free –OH vibration ($a_{\mathrm{F,–OH}}$) is determined from the reported values of free –OH concentration, absorbance, and film thickness of PVPh [33] and is used for all copolymer and composite systems.

In the nanotube–polymer composite system, the associated –OH group can be separated into contributions from the intra-associated –OH group and the inter-associated –OH group. The total –OH in the composite system is thus, given as

$$C_{\mathrm{T,–OH}} = C_{\mathrm{F,–OH}} + C_{\mathrm{I,–OH}} + C_{\mathrm{A,–OH}} \tag{5}$$

Where $C_{\mathrm{I,–OH}}$ is the concentration of hydrogen bonded –OH via inter-association and $C_{\mathrm{A,–OH}}$ is the concentration of hydrogen bonded –OH via intra-association. The values for $C_{\mathrm{I,–OH}}$ and $C_{\mathrm{A,–OH}}$ are calculated from

$$C_{\mathrm{I,–OH}} = \frac{A_{\mathrm{I,–OH}}}{(a_{\mathrm{asso,–OH}}b)} \tag{6}$$

$$C_{\mathrm{A,–OH}} = \frac{A_{\mathrm{A,–OH}}}{(a_{\mathrm{asso,–OH}}b)} \tag{7}$$

respectively, where $A_{\mathrm{I,–OH}}$ and $A_{\mathrm{A,–OH}}$ are determined experimentally from the FTIR spectra and the fitting process. Due to the overlap of the inter- and intra-associated –OH peaks, it was assumed that the absorption coefficients for inter- and intra-associated –OH are the same. Since, the values of the absorption coefficients and thickness are the same in Eqs. (6) and (7), the

ratio $C_{I,-OH}/C_{A,-OH}$ is equal to $A_{I,-OH}/A_{A,-OH}$. Normalizing the values of $A_{I,-OH}$ and $A_{A,-OH}$ to 1, the concentration of inter- and intra-associated –OH can than be calculated by multiplying the normalized absorbance of inter- and intra-associated –OH to the concentration of associated –OH, respectively.

The assumption that the absorption coefficients for inter- and intra-associated –OH are the same is a potential source of error in quantifying the –OH concentration and for this reason, the values that emerge from this analysis can only be used to compare the data presented here, and the values presented do not indicate an absolute measure of the percent –OH that are free or hydrogen bonded in each sample.

3.4.1. PSVPh–SWNT composites

The fitting of the experimentally determined FTIR curves to the deconvoluted peaks for one of the composites, the PSVPh30–SWNT nanocomposite is shown in Fig. 8. The results of the peak deconvolution and fitting process for the PSVPh–SWNT composites are plotted in Fig. 9. In the case of composites, the associated –OH peak is resolved into two peaks, namely that of the intra-associated hydrogen bonded –OH and the inter-associated hydrogen bonded –OH. The intra-associated –OH peak originates due to the interaction of –OH groups among polymer chains, however, the inter-associated –OH peak relates to the hydrogen bonding interaction of the –OH group of the polymer chain to functional groups on the SWNT.

The IR demonstrates that the nanocomposite with the copolymer that has 20% vinyl phenol has the most hydrogen bonding interactions between the nanotube and polymer, which correlates very well with the tensile test results for the composite systems. This agreement of trends between FTIR data and tensile data indicates that increasing inter-molecular hydrogen bonding between the copolymer and SWNT results in enhanced mechanical strength.

3.4.2. PSVPh–MWNT composites

The peak deconvolution and fitting results for the PSVPh–MWNT composites are plotted in Fig. 10. In general, the trends for the contribution of the free, inter and intra-associated –OH groups to the hydroxyl peak in the PSVPh–MWNT composites are similar to PSVPh–SWNT composites. The trends also reasonably compare with the tensile test results for PSVPh–MWNT composites.

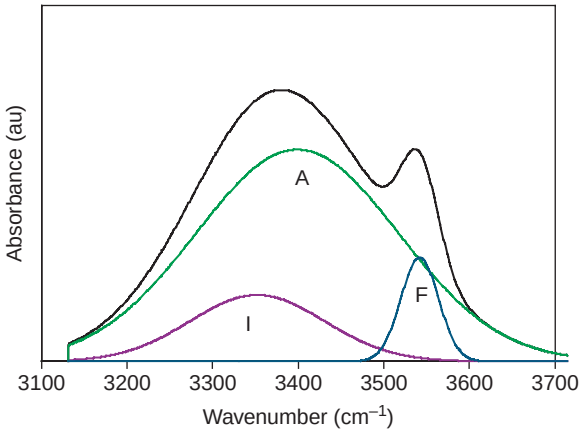

Fig. 8. Example of fitting and deconvolution procedure for and PSVPh30–SWNT. The curves F, A and I are deconvoluted peaks assigned for free, intra- and inter-associated OH bonds, respectively, obtained from the fit.

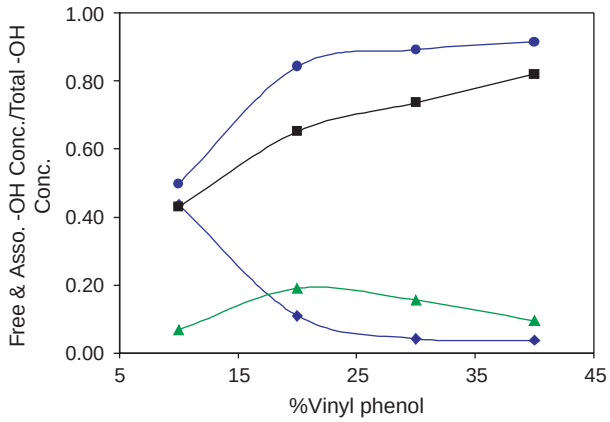

Fig. 9. Dependence of calculated concentration of free OH to total OH, $C_{F,-OH}/C_{T,-OH}$ (♦), associated OH to total OH, $C_{asso,-OH}/C_{T,-OH}$ (●), intra-associated OH to total OH, $C_{A,-OH}/C_{T,-OH}$ (■) and inter-associated OH to total OH, $C_{I,-OH}/C_{T,-OH}$ (▲) on % vinyl phenol for PSVPh–SWNT composites.

3.5. Discussion

The dependence of the contribution of the free, intra- and inter-associated –OH to the hydroxyl peak in the FTIR spectra of the nanocomposites on the composition of the copolymer and its correlation to the tensile properties of the nanocomposites can be explained in terms of accessibility of the OH [27,28,39] on the copolymer chain to participate in hydrogen bonding with the oxygenated functional groups on the nanotube. The PSVPh copolymer is a random copolymer. For a copolymer with a vinyl phenol content as low as 10%, both free and intra-associated –OH groups exist. However, at this vinyl phenol content, insufficient free –OH groups are available to interact with the defect sites of the SWNT. This

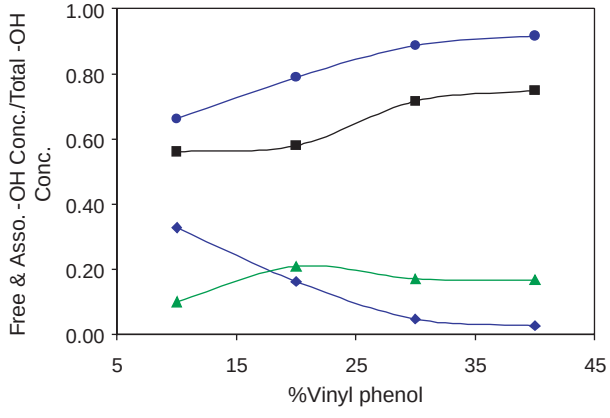

Fig. 10. Dependence of calculated concentration of free OH to total OH, $C_{F,-OH}/C_{T,-OH}$ (♦), associated OH to total OH, $C_{asso,-OH}/C_{T,-OH}$ (●), intra-associated OH to total OH, $C_{A,-OH}/C_{T,-OH}$ (■) and inter-associated OH to total OH, $C_{I,-OH}/C_{T,-OH}$ (▲) on % vinyl phenol for PSVPh–MWNT composites.

lack of sufficient vinyl phenol groups limits the extent to which the polymer chain can hydrogen bond with the SWNT. This is exemplified in the IR peak analysis, which shows a small contribution from inter association (0.08) for the PSVPh10–SWNT nanocomposite. As the content of vinyl phenol on the polymer backbone increases, the amount of hydroxyl group that can interact with the nanotube increases, and the analysis of the FTIR data indicates that this indeed occurs.

However, as the amount of hydroxyl groups increases the average distance between vinyl phenol moieties decreases. At some increased vinyl phenol content, the separation between two vinyl phenol groups becomes sufficiently small to promote interaction among hydroxyl groups via hydrogen bonding, or formation of intra-molecular hydrogen bond. Also, at higher hydroxyl concentration, where the separation of hydroxyls is limited, the presence of a hydrogen bond (intra or inter) can limit the dynamic mobility of neighboring hydroxyl groups on the same chain, thus limiting their ability to access and orient correctly for interaction with the functional groups on the nanotubes. Thus, at 30 and 40% vinyl phenol this crowding of –OH groups along the polymer chain limits their accessibility to form intermolecular interactions.

Thus, there must exist an optimum composition of the copolymer, where the –OH population is large enough to establish interaction between the copolymer and the carbon nanotubes but intra-molecular association is not strong enough to restrict the vinyl phenol groups on the copolymer chain to access the functional groups on the nanotube. From the tensile results, electrical conductivity, and FTIR analysis, it appears that the copolymer with 20% vinyl phenol corresponds to this optimum state.

4. Conclusions

The results presented in this paper clearly demonstrate that optimizing the extent of intermolecular interactions between a carbon nanotube and a polymer matrix provides a mechanism to improve the dispersion of the CNT in a polymer nanocomposite. The results also indicate that the improved CNT dispersion translates into improved mechanical and electrical properties. Nanocomposites of copolymers of styrene and vinyl phenol (PSVPh) with SWNT and MWNT were examined. Analysis of the FTIR data indicates that the polystyrene–vinyl phenol copolymer containing 20% vinyl phenol exhibits optimum amount of –OH groups that participate in intermolecular interactions between the polymer and the nanotube, which leads to the observed maximum improvement in tensile strength as well as the highest electrical conductivity. The results also show that the extent of interaction in a nanocomposite can be controlled by manipulating the amount of interacting groups on a copolymer chain.

Acknowledgements

A portion of this research was conducted at the Center for Nanophase Materials Sciences, which is sponsored at Oak Ridge National Laboratory by the Division of Scientific User Facilities, US Department of Energy. This research was also sponsored by the Division of Material Sciences and Engineering, Office of Basic Energy Sciences, US Department of Energy, under contract No. DE-AC05-00OR22725, managed and operated by UT-Battelle, LLC. We also acknowledge the financial support for this work from the National Science Foundation under Grant DMR-0241214.

References

[1] Lourie O, Wagner HD. J Mater Res 1998;13:2418–22.
[2] Calvert P. Nature 1999;399:210–1.
[3] Dresselhaus MS, Dresselhaus G, Saito R. Phys Rev B 1992;45:6234–42.
[4] Hone J, Llaguno MC, Biercuk MJ, Johnson AT, Batlogg B, Fischer JE. Appl Phys A 2002;74:339–43.
[5] Bower C, Rosen R, Jin L. Appl Phys Lett 1999;74:3317–9.
[6] Velasco-Santos C, Martinez-Hernandez AL, Fisher FT, Ruoff R, Castano VM. Chem Mater 2003;15:4470–5.
[7] Li S, Qin Y, Shi J, Guo Z, Li Y, Zhu D. Chem Mater 2005;17:130–5.
[8] Liu CH, Fan SS. Appl Phys Lett 2005;86:1231061–3.
[9] Guo H, Sreekumar TV, Liu T, Minus M, Kumar S. Polymer 2005;46:3001–5.
[10] Uchida T, Kumar S. J Appl Polym Sci 2005;98:985–9.
[11] Qian D, Dickey EC, Andrews R, Rantell T. Appl Phys Lett 2000;76:2868–70.
[12] Coleman JN, Balu WJ, Dalton AB, Munoz E, Collins S, Kim BG, et al. Appl Phys Lett 2003;82:1682–4.
[13] Sen R, Zhao B, Perea D, Itkis ME, Hu H, Love J, et al. Nano Lett 2004;4(3):459–64.
[14] Chae HG, Sreekumar TV, Uchida T, Kumar S. Polymer 2005;46:10925–35.
[15] Wood JR, Frogley MD, Meurs ER, Prins AD, Peijs T, Dunstan DJ, et al. J Phys Chem B 1999;103:10388–92.
[16] Wood JR, Zhao Q, Frogley MD, Meurs ER, Prins AD, Peijs T, et al. Phys Rev B 2000;62:7571–5.
[17] Cooper CA, Young RJ, Halsall M. Composites A 2001;32:401–11.
[18] Ajayan PM, Schadler LS, Giannaris C, Rubio A. Adv Mater 2000;12:750–3.
[19] Stephan C, Nguyen TP, Chapelle ML, Lefrant S, Journet C, Bernier P. Synth Met 2000;108:139–49.
[20] Zhang X, Liu T, Sreekumar TV, Kumar S, Moore VC, Hauge RH, et al. Nano Lett 2003;3:1285–8.
[21] Rasheed A, Dadmun MD, Britt PF, Geohegan D, Ivanov II. Chem Mater. Submitted for publication.
[22] Bower C, Rosen R, Jin L. Appl Phys Lett 1999;74:3317–9.
[23] Cooper AC, Cohen SR, Barber AH, Wagner HD. Appl Phys Lett 2002;81:3873–5.
[24] Barber AH, Cohen SR, Wagner HD. Appl Phys Lett 2003;82:4140–2.
[25] Poggi MA, Lillehei PT, Bottomley LA. Chem Mater 2005;17:4289–95.
[26] Poggi MA, Bottomley LA, Lillehei PT. Nano Lett 2004;4:61–4.
[27] Painter PC, Tang W-L, Graf JF, Thomson B, Coleman MM. Macromolecules 1991;24:3929–36.
[28] Coleman MM, Pehlert GJ, Painter PC. Macromolecules 1996;29:6820–31.
[29] Coleman MM, Lee KH, Skrovanek DJ, Painter PC. Macromolecules 1986;19:2149.
[30] Pedrosa P, Pomposo JA, Calahorra E, Cortozar M. Macromolecules 1994;27:102–9.
[31] Landry CJT, Massa DJ, Teegarden DM, Landry MR, Henrichs PM, Colby RH, et al. Macromolecules 1993;26:6299–307.
[32] Teegarden DM, Landry CJT. J Polym Sci, Part B: Polym Phys 1995;33:1933–43.
[33] Li D, Brisson J. Polymer 1998;39:793–800.
[34] Radmard B, Dadmun MD. Polymer 2001;42:1591–600.

[35] Eastwood E, Viswanathan S, O'Brien CP, Kumar D, Dadmun MD. Polymer 2005;46:3957.
[36] Viswanathan S, Dadmun MD. Macromolecules 2003;36:3196–205.
[37] Viswanathan S, Dadmun MD. Macromol Rapid Commun 2001;22: 779–82.
[38] Viswanathan S, Dadmun MD. Macromolecules 2002;35:5049–60.
[39] Viswanathan S, Dadmun MD. J Polym Sci, Polym Phys 2004;42: 1010–22.
[40] Bom D, Andrews R, Jacques D, Anthony J, Chen B, Meier MS, et al. Nano Lett 2002;2(6):615–9.
[41] Mawhinney DB, Naumenko V, Kuznetsova A, Yates Jr JT, Liu J, Smalley RE. Chem Phys Lett 2000;324:213–6.
[42] Colthup NB, Daly LH, Wiberley SE. Introduction to infrared and Raman spectroscopy. New York: Academic press; 1975.
[43] Li S, Qin Y, Shi J, Gou ZX, Li Y, Zhu D. Chem Mater 2005;17: 130–5.